Adsorption of Polyether Block Copolymers at Silica–Water and Silica–Ethylammonium Nitrate Interfaces

ARTICLE *in* LANGMUIR · JUNE 2015

Impact Factor: 4.46 · DOI: 10.1021/acs.langmuir.5b01500 · Source: PubMed

Langmuir

Article

pubs.acs.org/Langmuir

Adsorption of Polyether Block Copolymers at Silica–Water and Silica–Ethylammonium Nitrate Interfaces

Zhengfei Chen,[†] Yumi Kobayashi,[‡] Grant B. Webber,[†] Kazuhide Ueno,[§] Masayoshi Watanabe,[‡] Gregory G. Warr,[∥] and Rob Atkin*[,†]

[†]Newcastle Institute for Energy and Resources, The University of Newcastle, Callaghan, New South Wales 2308, Australia

[‡]Department of Chemistry and Biotechnology, Yokohama National University, 79-5 Tokiwadai, Hodogaya-ku, Yokohama 240-8501, Japan

[§]Department of Applied Chemistry, Faculty of Engineering, Yamaguchi University, 2-16-1 Tokiwadai, Ube, Yamaguchi 755-8611, Japan

[∥]School of Chemistry, The University of Sydney, Sydney, New South Wales 2006, Australia

Supporting Information

ABSTRACT: Atomic force microscope (AFM) force curves and images are used to characterize the adsorbed layer structure formed by a series of diblock copolymers with solvophilic poly(ethylene oxide) (PEO) and solvophobic poly(ethyl glycidyl ether) (PEGE) blocks at silica–water and silica–ethylammoniun nitrate (EAN, a room temperature ionic liquid (IL)) interfaces. The diblock polyethers examined are $EGE_{109}EO_{54}$, $EGE_{113}EO_{115}$, and $EGE_{104}EO_{178}$. These experiments reveal how adsorbed layer structure varies as the length of the EO block varies while the EGE block length is kept approximately constant; water is a better solvent for PEO than EAN, so higher curvature structures are found at the interface of silica with water than with EAN. At silica–water interfaces, $EGE_{109}EO_{54}$ forms a bilayer and $EGE_{113}EO_{115}$ forms elongated aggregates, while a well-ordered array of spheres is present for $EGE_{104}EO_{178}$. $EGE_{109}EO_{54}$ does not adsorb at the silica–EAN interface because the EO chain is too short to compete with the ethylammonium cation for surface adsorption sites. However, $EGE_{113}EO_{115}$ and $EGE_{104}EO_{178}$ do adsorb and form a bilayer and elongated aggregates, respectively.

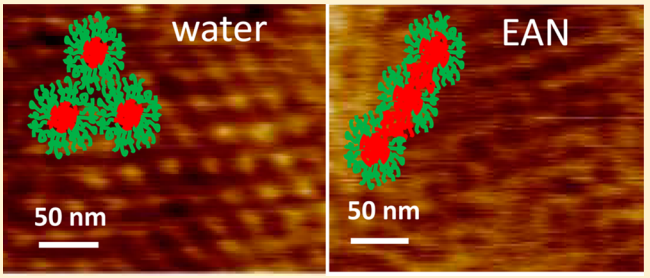

INTRODUCTION

Ionic liquids (ILs) are pure salts that are liquid below 100 °C. As a result of their many useful physical properties, ILs have attracted considerable research interest in a diverse range of fields including electrochemistry,[1,2] solar cells,[3,4] cellulose processing,[5] catalysis,[6−8] materials synthesis,[9,10] polymer science,[11,12] liquid–liquid extractions,[13,14] amphiphile self-assembly,[15−17] and environmental science.[18]

Ionic liquids are often classified as protic or aprotic according to the synthesis method. The most well studied protic IL is ethylammonium nitrate (EAN)[19] which has a melting point of 12 °C, relatively low viscosity, and good thermal stability.[20] Like many protic ILs, EAN has a three-dimensional hydrogen bond network[21,22] and well-defined bulk liquid nanostructure.[23] Protic IL nanostructure results from attractions (electrostatic and hydrogen bonding) between charged groups, leading to the formation of polar domains, from which cation alkyl chains are solvophobically excluded and cluster together to form apolar regions. In EAN these polar and apolar domains percolate through the bulk in a bicontinuous, sponge-like morphology.

Amphiphilic block copolymers are comprised of insoluble (solvophobic) and soluble (solvophilic) blocks. In bulk solution, when the critical aggregation concentration (cac) is exceeded, they self-assemble into various structures with their solvophobic groups sequestered in a core and solvophilic groups in contact with the solvent,[24] similar to conventional surfactant micelles.[25,26] However, because block copolymers have much higher molecular weights than surfactants, block copolymer micelles are often less dynamic.[27] Packing constraints on the relative lengths of the soluble and insoluble blocks determine the block copolymer micelle shape.[24] In water, large micelles form when the mass fraction of the hydrophilic block is less than 25%, and spherical micelles arise for hydrophilic mass fractions of more than 45%. Between these two compositions a wide variety of structures such as disks, rods, and vesicles form. The properties of block copolymer aggregates can be tuned by varying the block length or monomer unit type, and as a result they have attracted considerable research interest for drug delivery[28,29] and materials synthesis,[30,31] as well as many other areas.[27]

Received: April 26, 2015
Revised: June 2, 2015
Published: June 3, 2015

DOI: 10.1021/acs.langmuir.5b01500
Langmuir 2015, 31, 7025−7031

Conventional low molecular weight surfactants tend to have high solubilities in ILs because the IL apolar domains increase the solubility of tail groups compared to water.[16,32] This results in higher critical micelle concentrations in ILs, and therefore reduced surfactant efficiency.[15] This can be partially offset by increasing the surfactant tail length to increase solvophobicity. However, longer alkyl chain surfactants also have higher Krafft temperatures; surfactants with alkyl chains C_{18} or longer are usually insoluble at room temperature.[33] Furthermore, conventional surfactants do not adsorb at the interface between ILs and charged surfaces. This is because the IL ions are smaller than the surfactant headgroups, and are present at a much higher concentration, so preferentially bind to surface adsorption sites. This means that interfacial properties in ILs cannot be modified using conventional surfactants in ILs in the same way as in water.

For these reasons, several groups have recently examined the behavior of amphiphilic block copolymers in ILs.[34−43] Solvophobic groups in amphiphilic block copolymers are usually bulkier (e.g., poly(propylene oxide), PPO) than the saturated hydrocarbon chains used in conventional surfactants. This means they are less readily solubilized by IL apolar domains, leading to lower cac's and higher efficiency. Block copolymers also tend not to crystallize,[40] so their solubility remains high[44] unlike convention surfactants. Nonionic block copolymers are often used in ILs because electrostatic attractions between IL ions and the monomer units of ionic block copolymer frequently results in insolubility.

A popular class of nonionic block copolymers is Pluronic triblock copolymers, which are composed of hydrophilic poly(ethylene oxide) (PEO) blocks and hydrophobic propylene oxide (PPO) blocks.[45−47] Self-assembly of Pluronics into micelles and liquid crystals has been reported in EAN,[35,48,49] and we have described the adsorbed layer structure of three Pluronics (P65, L81, L121) at the silica−EAN interface.[48] AFM imaging revealed that EO rich P65 ($EO_{19}PO_{30}EO_{19}$) adsorbed in a mushroom-like conformation structurally similar to the P65 micelles in bulk EAN elucidated using small angle neutron scattering (SANS).[48] L81 ($EO_3PO_{43}EO_3$) adsorbed in a laterally featureless brush conformation, consistent with its short EO groups favoring low curvature structures, but L121 ($EO_5PO_{68}EO_5$) did not adsorb at the silica−EAN interface. SANS indicated that L121 formed a vesicle dispersion at room temperature, and contact mode AFM force curves suggested that nonadsorbed lamellae were present near the surface. To the authors' knowledge this is the only study of block copolymer adsorption at solid−IL interfaces. This is in contrast to Pluronic adsorption at solid−aqueous interfaces which are better characterized. For example, when the Pluronic concentration exceeds the cac, P105 ($EO_{37}PO_{56}EO_{37}$) forms spherical aggregates on silica nanoparticles[50] and silica surfaces.[51] The structure of PPO−PEO diblock copolymers has also been probed at aqueous interfaces. Hamley et al. studied the adsorption of $PO_{94}EO_{316}$ from water on both silica and mica by AFM imaging and revealed an adsorbed layer of spherical adsorbed micelles whose surface packing density increased with polymer concentration.[52]

In this work AFM imaging and force curves are used to compare the structures of novel block copolymers adsorbed at silica−water and silica−EAN interfaces. The block copolymers are nonionic diblock polyethers with hydrophilic PEO blocks and hydrophobic poly(ethyl glycidyl ether) (PEGE) blocks, abbreviated EGE_mEO_n. PEGE is structurally similar to PPO but with an ethyl ether moiety added to the monomer unit which increases the oxygen content and the bulkiness of the solvophobic chain. PEGE has lower oxygen content than PEO[53] and is sufficiently solvophobic to promote the self-assembly of EGE_mEO_n polyethers in water[54] as well as in ILs.[55,56] The block copolymers examined here are $EGE_{109}EO_{54}$, $EGE_{113}EO_{115}$, and $EGE_{104}EO_{178}$. Since the length of the solvophobic EGE block is approximately constant while the EO block length changes, these experiments reveal how changing the EO length effects adsorbed structures at the silica−water and silica−EAN interfaces, and comparison of results for the same polymer in EAN and water elucidate how the solvent influences adsorbed structure.

We have recently reported the *bulk phase* aggregate structures of the same block copolymers in EAN and water.[56] As is commonly found for block copolymers in various solvents,[37,43] the aggregate shapes were determined by the ratio of the solvophilic and solvophobic block lengths. $EGE_{109}EO_{54}$, which has the shortest EO block, formed planar shapes in both water and EAN. When the EO chain length was increased in $EGE_{113}EO_{115}$, higher curvature spherical aggregates were observed in water but disks were still present in EAN. This is a consequence of EAN being a poorer solvent for PEO than water,[57] meaning that EO groups are less well solvated which favors lower curvature structures. When the EO content was further increased in $EGE_{104}EO_{178}$, spherical structures were retained in water. In EAN this concentration was *just* above the cac, due to the long EO chain increasing the solubility of individual chains.[56] The low aggregate volume fraction resulted in weak scattering which meant that structures could not be determined unequivocally.

EXPERIMENTAL SECTION

Materials. EAN was prepared by slowly mixing equimolar acid (69 wt % HNO_3, BASF) and base (ethylamine, 70 wt %, Sigma-Aldrich) under chilled conditions. The excess water was mostly removed by rotary evaporation at 40 °C for several hours which resulted in water content less than 1 wt %. Residual water was removed by purging the EAN with nitrogen gas at 105 °C in an oil bath for at least 8 h. The water content of the EAN used was undetectable by Karl Fisher titration (<0.01%).

The molecular structures of the EGE_m and EO_n blocks are shown in Figure 1, where *m* and *n* denote respectively the number of EGE and EO units. Three polyethers with various fractions of PEO were synthesized as previously reported,[53] with the molecular weights (M_n) and polydispersity indexes (PDI) presented in Table 1. The approximate fully extended lengths of the diblock copolymer backbones, based on bond lengths, are $EGE_{109}EO_{54}$ = 82 nm, $EGE_{113}EO_{115}$ = 114 nm, and $EGE_{104}EO_{178}$ = 141 nm.

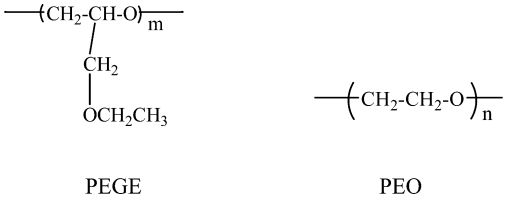

Figure 1. Molecular structures of the solvophobic PEGE and solvophillic PEO repeat units.

Sample Preparation. Polymer/water and polymer/EAN samples with various polymer concentrations (0.1 and 1 wt %) were stirred overnight in a sealed glass vial at room temperature prior to measurements. The substrates for all adsorption experiments were commercial (001) silicon wafers with a 130 nm thick thermally grown

DOI: 10.1021/acs.langmuir.5b01500
Langmuir 2015, 31, 7025−7031

Table 1. Polyether Amphiphile Composition, Molecular Weight (M_n) and Polydispersity Index (PDI)

			total	
polyether	no. of EGE units	no. of EO units	M_n	PDI
$EGE_{109}EO_{54}$	109	54	13600	1.16
$EGE_{113}EO_{115}$	113	115	16700	1.24
$EGE_{104}EO_{178}$	104	178	18600	1.32

oxide layer. The substrates were immersed in 0.1 M HCl solution overnight and then were cleaned with distilled water and ethanol and blown dry with a nitrogen stream. The surface was exposed to ultraviolet light for 20 min prior to the AFM experiment.

Atomic Force Microscopy. AFM soft-contact imaging and normal force curve measurements were performed on a Nanoscope VIII Multimode (Bruker, Billerica, MA, USA). Conventional sharp cantilevers with a manufacturer-quoted spring constant of approximately 0.06 N/m were used throughout. AFM experiments were performed using a sealed fluid cell. Each solution was injected into the cell and allowed to equilibrate for 20 min prior to measurements. Prior to injecting a solution the cleanliness of the silica surface was confirmed by force curves and images recorded in air. Repeat experiments were completed on at least 3 different days. For force curves, there was some variability in the magnitude of the measured forces (±15%) on different days, but the separations at which features were noted (that are key to our intepretations) were consistent. The relative velocity of the cantilever during both approach and retraction was maintained at 40 nm/s. This low speed minimized potential fluid dynamic effects during measurement. The appearance of AFM images over repeat experiments was consistent.

RESULTS AND DISCUSSION

In this work we seek to probe the structure of the diblock copolymer at the silica−water and silica−EAN interfaces when the surface is saturated. Typically the saturation surface excess occurs when the bulk amphiphile concentration is ∼2/3 × cac,[51] so we have studied concentrations slightly above the cac: 0.1 wt % for water and 1 wt % for EAN.

Adsorption at the Water−Silica Interface. Typical force data for the approach and retraction of the AFM tip to a silica surface immersed in 0.1 wt % $EGE_{109}EO_{54}$ is shown in Figure 2.

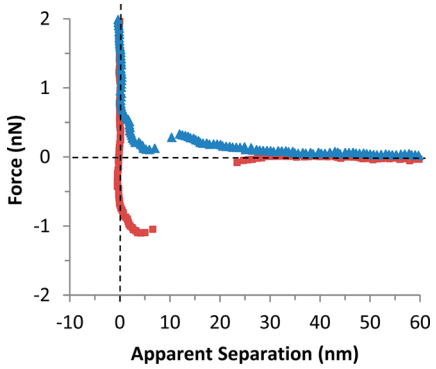

Figure 2. Force−distance profile for 0.1 wt % $EGE_{109}EO_{54}$ at the silica−water interface: triangles, approach; squares, retraction.

A gentle repulsion is measured from a separation of about 35 nm. The repulsion increases more rapidly with distance from ∼16 nm until a push through occurs at 12.5 nm whereupon the tip jumps to 7 nm and a second, steeper repulsion occurs. A second push through occurs at 2 nm, and the tip moves into compliance; this final push through was present in ∼90% of force curves. When the tip is retracted from the surface, an adhesion occurs to a separation of 5 nm, at which point the tip jumps back to zero force. AFM images of this system were featureless (not shown).

The SANS data for $EGE_{109}EO_{54}$ in water revealed that bilayer structures (vesicles or very large disks) were present in the bulk.[56] The thickness of the EGE core was 11 nm, but the EO layer thickness could not be determined from SANS because it was so highly solvated by water (D_2O), resulting in low scattering contrast. The AFM data presented in Figure 2 are consistent with a similar bilayer structure adsorbed to the silica surface. The gentle repulsion from 35 to 16 nm is due to weak steric interactions between distal chains bound to the surface and the tip. At 16 nm, the tip comes into contact with solution facing EO groups of $EGE_{109}EO_{54}$ in the surface bilayer. These are compressed over ∼2 nm, at which point the force applied by the AFM tip is sufficient to displace $EGE_{109}EO_{54}$ in contact with solution, and the tip jumps into contact with the $EGE_{109}EO_{54}$ layer that is bound to the silica surface. Given the bulk structure, and the fact that EO will have higher affinity for hydrogen bonding sites on the silica surface than EGE (it is less sterically constrained), it is expected that $EGE_{109}EO_{54}$ in the surface layer will predominantly be adsorbed with EO groups in contact with the silica and EGE facing solution. From 7 nm the tip pushes against this layer and compresses it. The final push through at 2 nm is likely to be the tip displacing the surface bound layer and moving into contact with the silica surface. The form of the retraction data is consistent with extension and detachment of a polymer chain that bridges between the AFM tip and the surface in a good solvent.[58]

It is probable that the EO layer in contact with the silica is somewhat thinner than the outward facing layer, as it adsorbs along the substrate in loops and trains; the final push through suggests the EO layer in contact with the surface is of 2 nm. If the EGE core is 11 nm wide, consistent with the bulk aggregate, the EO layer in contact with it is 4 nm thick. The EO shell thickness determined for $EGE_{113}EO_{115}$ micelles was 7 nm,[56] so a thickness of 4 nm for solution facing EO_{54} is reasonable.

Force data and a typical AFM image for the interface of silica with 0.1 wt % $EGE_{113}EO_{115}$ in water are shown in Figure 3. The

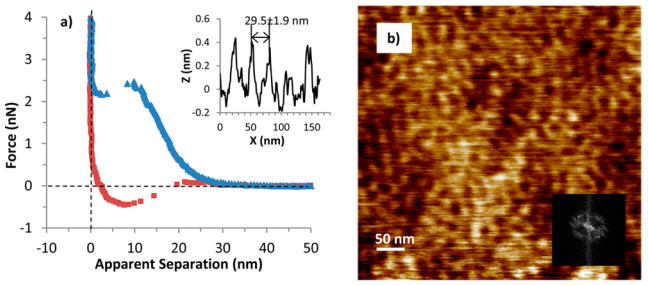

Figure 3. Force−distance profile (a), soft-contact image (b), and a section analysis and the two-dimensional Fourier transform (inset) from the image for 0.1 wt % $EGE_{113}EO_{115}$ at the silica−water interface.

substantial increase in the length of the EO block leads to markedly different features for $EGE_{113}EO_{115}$ compared to $EGE_{109}EO_{54}$ and is consistent with the different bulk structures. The approach force increases nonlinearly between 31 and 22 nm and then increases linearly to 10 nm before jumping to compliance; linear increases in force with compression have been observed previously for adsorbed micelles.[52] A weak adhesion is present on retraction that extends to ∼10 nm before the tip snaps back to zero force at 20 nm. The soft-

DOI: 10.1021/acs.langmuir.5b01500
Langmuir 2015, 31, 7025−7031

contact AFM image (Figure 3b) reveals a layer of aggregates adsorbed to the silica surface. The lateral nearest-neighbor separation of the adsorbed aggregates is approximately 30 nm from both the Fourier transform (inset Figure 3b) and several section analyses, an example of which is shown in Figure 3. When high force was applied during imaging, the adsorbed polymer layer was pushed through, revealing the silica surface (Supporting Information (SI) Figure S1). This suggests that the compliance region in the force curve corresponds to tip−silica contact.

In bulk aqueous solution $EGE_{113}EO_{115}$ forms spherical core−shell micelles. The EGE core radius is 13 nm and the PEO shell is 7 nm thick, giving an overall micelle diameter of 40 nm. This is one-third larger than the adsorbed aggregate diameter (i.e., nearest-neighbor closest-packing separation) suggested by the AFM images, and the adsorbed layer thickness derived from the force curve (if it is assumed that compliance means tip−silica contact), both of which are 30 nm. This is a consequence of attractions between the EO blocks and the silica surface, and surface coalescence and packing. When a micelle adsorbs, hydrogen bonding between EO groups and the silica surface leads to the formation of loops and trains and the micelle spreads across the substrate, resulting in a thinner PEO layer on the substrate and an overall flatter structure. The smaller lateral dimension is a consequence of the micelles being tightly packed when surface adsorption sites are saturated. Such close proximity leads to intercalation of the EO groups of neighboring micelles resulting in smaller effective diameters than a dilute micelle in bulk solution.[52] In much of the image, several aggregates are poorly resolved or appear to have merged (at least partially) together.

Figure 4 shows the normal force data and AFM soft-contact image for a silica surface immersed in a 0.1 wt % aqueous

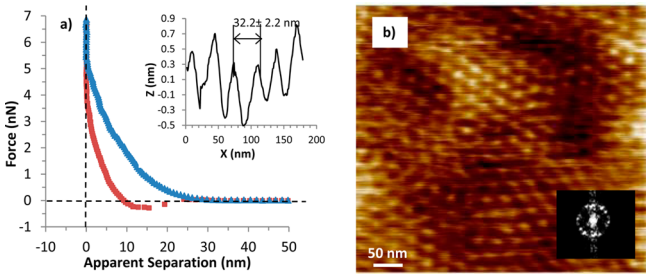

Figure 4. Force−distance profile (a), soft-contact image (b), and a section analysis and the two-dimensional Fourier transform (inset) from the image for 0.1 wt % $EGE_{104}EO_{178}$ at the silica−water interface.

solution of $EGE_{104}EO_{178}$. In contrast to the force data for $EGE_{109}EO_{54}$ and $EGE_{113}EO_{115}$, there are no push throughs and a purely compressive force is measured from a separation of 25 nm on approach, with minimal adhesion on retraction. This shows that the AFM tip is unable to rupture the polymer layer and move into contact with the silica, and as such the compliance region in the force curve corresponds to the tip in contact with a compressed polymer film; for this system high force AFM images did not reveal the silica surface. The inability of the AFM tip to rupture the $EGE_{104}EO_{178}$ layer is in contrast to results for $EGE_{109}EO_{54}$ and $EGE_{109}EO_{115}$ and attributed to the longer EO group making more surface attachments per block copolymer, which increases the strength of binding.

The AFM image in Figure 4 reveals an adsorbed layer of spherical, hexagonally well-packed, uniform size micelles. The Fourier transform is a well-defined ring which reveals the interaggregate spacing is ∼32 nm, as does the section analysis. SANS showed that in solution $EGE_{104}EO_{178}$ forms high curvature spherical micelles with a diameter of 38 nm,[56] consisting of a 18 nm EGE core within a 10 nm thick EO shell. Like that for $EGE_{113}EO_{115}$, the surface interaggregate spacing is less than the bulk micelle diameter due to steric interactions between the EO groups of micelles densely adsorbed on the surface. In contrast to $EGE_{113}EO_{115}$ the aggregates are discrete with almost no evidence of coalescence of neighboring micelles. This is attributed to the longer EO group enhancing steric interactions which prevents contact between the EGE cores of neighboring micelles.

Adsorption at the EAN−Silica Interface. Force data for the interface of silica with pure EAN has been reported previously[43,56] and consists of three or four steps 0.5 nm apart. Pure EAN is 11.2 M in ionic strength which completely screens the charge on the silica surface and the tip allowing the structural forces associated with near-surface liquid layers to be measured. Near a solid surface, the bulk sponge-like nanostructure of EAN transforms into flatter structures[59] that produce the 0.5 nm steps (which is equal to the EAN ion pair dimension[60]) as they are expelled from the space between the tip and the surface. Electrostatic attractions between cations and the surface mean that the ion layer in contact with the silica is cation rich.[60]

The force data for 1 wt % $EGE_{109}EO_{54}$ at the silica EAN interface (Figure 5) is unlike any of the aqueous systems

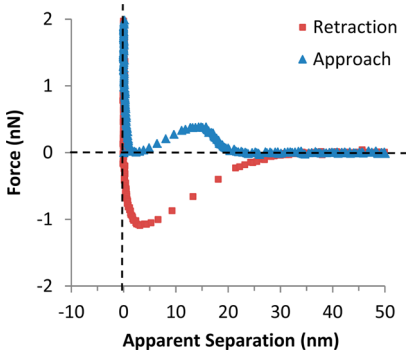

Figure 5. Force−distance profile for 1 wt % $EGE_{109}EO_{54}$ at the silica−EAN interface: triangles, approach; squares, retraction.

examined. A repulsion is measured from a separation of ∼20 nm which reaches a maximum at 15 nm, at which point a jump (attraction) occurs and the force returns to 0 at 2 nm separation before moving into compliance. AFM images for this system were the same as images of the silica substrate immersed in EAN.

This type of force curve has been observed previously for solutions of $C_{16}E_6$ in EAN and was attributed to the expulsion of near-surface (nonadsorbed) micelles from between the surface and the tip on approach.[48] SANS revealed that $EGE_{109}EO_{54}$ forms a bilayer in bulk EAN at this concentration with an EGE core thickness of 13 nm. The EO layer thickness could not be determined due to weak contrast with the solvent.

Thus, the force data in Figure 5 likely corresponds to the AFM tip rupturing or pushing aside a nonadsorbed $EGE_{109}EO_{54}$ bilayer near the surface. From the force data alone, it is difficult to tell whether the bilayer was initially present near the surface or simply somewhere between tip and

DOI: 10.1021/acs.langmuir.5b01500
Langmuir 2015, 31, 7025−7031

substrate until it was dragged to the substrate by the approaching AFM tip. The absence of any longer range repulsions suggests that the bilayer was most likely already near the surface and may be weakly attached. The width of the oscillation (18 nm) is consistent with a 13 nm EGE core surrounded by an ∼2.5 nm thick EO shell. The adhesion noted on retraction of the tip is likely osmotic in origin, as the membrane cannot fill the space between the tip and the surface until the separation is sufficiently wide.

$EGE_{109}EO_{54}$ adsorbed to the silica−water interface in a bilayer conformation but does not adsorb at the silica−EAN interface. This is attributed to the ethylammonium cations having higher affinity for negatively charged sites on the silica surface than water. This limits the number of hydrogen bonds that can form between the short EO_{54} block and the surface, which prevents adsorption.

AFM force−distance data for the interface of silica with 1 wt % $EGE_{113}EO_{115}$ in EAN is presented in Figure 6. The force

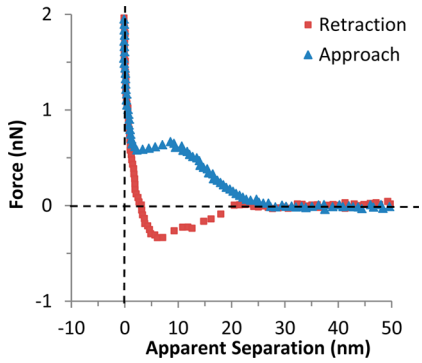

Figure 6. Force−distance profile for 1 wt % $EGE_{113}EO_{115}$ at the silica−EAN interface: triangles, approach; squares, retraction.

increases from a separation of 25 nm followed by a push through at 10 nm whereupon the tip jumps in to 2 nm. A small compression then occurs before the tip moves into compliance. On retraction an adhesion occurs to a separation of ∼7 nm when the tip jumps back to zero force. AFM images were featureless (not shown).

These data clearly indicate that polymer is adsorbed to the silica. The finding that $EGE_{113}EO_{115}$ adorbs to the silica in the presence of EAN when $EGE_{109}EO_{54}$ does not is attributed to the longer EO group providing a greater number of attachment points per monomer. The form of the force data for $EGE_{113}EO_{115}$ in EAN is similar to that presented in Figure 2 for $EGE_{109}EO_{54}$ in water, where an adsorbed bilayer was present. This is consistent with bilayer structures being present in the bulk in both systems[56] which, combined with the featureless AFM image, suggests an adsorbed bilayer is also present on silica for the $EGE_{113}EO_{115}$ in EAN. Higher curvature elongated aggregates were found in water (Figure 3) for $EGE_{113}EO_{115}$. EAN is a poorer solvent for PEO than water, which means that the EO chains are less extended which favors flatter structures.

For $EGE_{109}EO_{54}$ in water, a second small push through was noted at short separations which suggested that the block copolymer was displaced and the tip moved into contact with the surface. A similar second push through is not seen here, meaning that a compressed polymer film remains in place up to high force. This is different from $EGE_{113}EO_{115}$ in water, which was displaced at high loads to reveal the silica substrate. As adsorption should generally be weaker in EAN due to higher solubility of the EGE block and competition from the cation for surface adsorption sites, this difference is attributed to EAN being 30 times more viscous than water. Increased viscosity prevents the polymer film from moving out of the space between the tip and the surface on the time scale of the experiment.

The absence of the second push through makes it impossible to estimate the thickness of the silica facing EO shell. SANS suggested that the EGE core for $EGE_{113}EO_{115}$ in EAN was 16 nm thick but the shell thickness could not be determined because of low contrast. If it is assumed that the thickness of the EGE layer at the silica interface is similar, the total width of the solution facing and silica facing EO shells must be at least 9 nm.

Force curves and AFM image for the interface of 1 wt % $EGE_{104}EO_{178}$ in EAN are shown in Figure 7. For comparison an

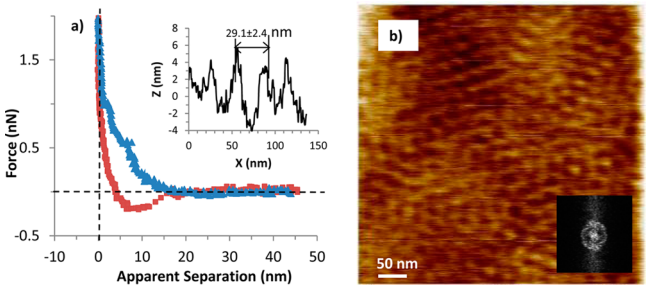

Figure 7. Force−distance profile (a), soft-contact image (b), and a section analysis and the two-dimensional Fourier transform (inset) from the image for 1 wt % $EGE_{104}EO_{178}$ at the silica−EAN interface.

image of the bare silica−EAN interface is given in Figure S2 (Supporting Information). The image reveals a surface saturated by a poorly resolved array of globular aggregates, strikingly similar to $EGE_{113}EO_{115}$ in water, and is likewise attributed to coalescence of micelles on the surface. This occurs for $EGE_{104}EO_{178}$ in EAN but not in water because EO chains are less extended in EAN. This means that steric repulsions between micelles on the surface are weaker, permitting contact between EGE. The small nearest-neighbor distances between surface $EGE_{104}EO_{178}$ aggregates in EAN (29 nm) and water (32 nm) is also attributed to EO chains being less extended in EAN than water and surface packing.

The force curve for $EGE_{104}EO_{178}$ at the silica−EAN interface reveals a repulsive compression that begins at ∼20 nm and continues until compliance is reached, with no evidence of a push through, and AFM images at high force did not reveal the silica surface. This shows that the block copolymer remains adsorbed to the surface at high force, similar to $EGE_{104}EO_{178}$ in water, revealing that the long EO chain leads to many attachment points and strong adsorption in EAN. The weak adhesion noted on retraction is consistent with extension of a polymer chain that bridges between the tip and the surface before breaking away.

■ CONCLUSIONS

Block copolymers are attractive additives for modifying the properties of solid−liquid interfaces. Provided the length of the adsorbing block is sufficient, they adsorb strongly to solid surfaces, and the capacity to vary the compositions and lengths of the soluble and insoluble blocks enables a high degree of

DOI: 10.1021/acs.langmuir.5b01500
Langmuir 2015, 31, 7025−7031

control over adsorbed structures and properties. In this work we have studied the adsorption of three novel amphiphilic polyethers at the silica−water and silica−EAN interfaces and shown that the structures present depend on both the block copolymer and solvent. This is of key importance for interfaces between ILs and charged substrates because conventional surfactants do not adsorb as they are unable to compete effectively for surface adsorption sites.

At silica−water interfaces, as in the bulk, the curvature of the adsorbed polyether structures increases as the EO length is increased: a laterally featureless bilayer is present for $EGE_{109}EO_{54}$, elongated aggregates are present for $EGE_{113}EO_{115}$, and spherical micelles are present for $EGE_{104}EO_{178}$. When high force was applied to the AFM tip, $EGE_{109}EO_{54}$ and $EGE_{113}EO_{115}$ were displaced from the silica surface but $EGE_{104}EO_{178}$ remained bound. This is attributed to the longer EO group providing a greater number of attachment points per monomer resulting in stronger adsorption.

EAN is a poorer solvent for PEO than water, which leads to lower curvature structures in the bulk and at the interface when adsorption occurs. The force data for $EGE_{109}EO_{54}$ at the EAN silica interface suggests a bilayer near to, but not adsorbed on, the surface, which the AFM tip ruptures on approach. This shows that the EO_{54} chain is too short to compete effectively with EAN for surface adsorption sites. $EGE_{113}EO_{115}$ does adsorb at the EAN−silica interface and forms a bilayer structure like that found for $EGE_{109}EO_{54}$ in water, and $EGE_{104}EO_{178}$ forms elongated aggregate like $EGE_{113}EO_{115}$ in water. These differences are attributed to poorer solvation of the EO chain in EAN than in water.

■ ASSOCIATED CONTENT

Supporting Information

Figures showing AFM images of 0.1 wt % $EGE_{104}EO_{178}$ at the silica−water interface and of the bare silica−EAN interface. The Supporting Information is available free of charge on the ACS Publications website at DOI: 10.1021/acs.langmuir.5b01500.

■ AUTHOR INFORMATION

Corresponding Author

*E-mail: rob.atkin@newcastle.edu.au.

Notes

The authors declare no competing financial interest.

■ ACKNOWLEDGMENTS

This research was supported by an Australian Research Council Discovery Project (DP130102298). R.A. thanks the Australian Research Council Future Fellowship (FT120100313).

■ REFERENCES

(1) Howlett, P. C.; Izgorodina, E. I.; Forsyth, M.; MacFarlane, D. R. Electrochemistry at negative potentials in bis-(trifluoromethanesulfonyl)amide ionic liquids. *Z. Phys. Chem.* **2006**, *220*, 1483−1498.

(2) Macfarlane, D. R.; Forsyth, M.; Howlett, P. C.; Pringle, J. M.; Sun, J.; Annat, G.; Neil, W.; Izgorodina, E. I. Ionic liquids in electrochemical devices and processes: Managing interfacial Electrochemistry. *Acc. Chem. Res.* **2007**, *40*, 1165−1173.

(3) Mazille, F.; Fei, Z. F.; Kuang, D. B.; Zhao, D. B.; Zakeeruddin, S. M.; Gratzel, M.; Dyson, P. J. Influence of ionic liquids bearing functional groups in dye-sensitized solar cells. *Inorg. Chem.* **2006**, *45*, 1585−1590.

(4) Rong, Y.; Ku, Z.; Xu, M.; Liu, L.; Hu, M.; Yang, Y.; Chen, J.; Mei, A.; Liu, T.; Han, H. Efficient monolithic quasi-solid-state dye-sensitized solar cells based on poly(ionic liquids) and carbon counter electrodes. *RSC Adv.* **2014**, *4*, 9271−9274.

(5) Pinkert, A.; Marsh, K. N.; Pang, S. S.; Staiger, M. P. Ionic Liquids and Their Interaction with Cellulose. *Chem. Rev.* **2009**, *109*, 6712−6728.

(6) Parvulescu, V. I.; Hardacre, C. Catalysis in ionic liquids. *Chem. Rev.* **2007**, *107*, 2615−2665.

(7) Welton, T. Ionic liquids in catalysis. *Coord. Chem. Rev.* **2004**, *248*, 2459−2477.

(8) van Rantwijk, F.; Sheldon, R. A. Biocatalysis in ionic liquids. *Chem. Rev.* **2007**, *107*, 2757−2785.

(9) Cooper, E. R.; Andrews, C. D.; Wheatley, P. S.; Webb, P. B.; Wormald, P.; Morris, R. E. Ionic liquids and eutectic mixtures as solvent and template in synthesis of zeolite analogues. *Nature* **2004**, *430*, 1012−1016.

(10) Jacob, D. S.; Joseph, A.; Mallenahalli, S. P.; Shanmugam, S.; Makhluf, S.; Calderon-Moreno, J.; Koltypin, Y.; Gedanken, A. Rapid Synthesis in Ionic Liquids of Room-Temperature-Conducting Solid Microsilica Spheres. *Angew. Chem., Int. Ed.* **2005**, *44*, 6560−6563.

(11) Lu, J.; Yan, F.; Texter, J. Advanced applications of ionic liquids in polymer science. *Prog. Polym. Sci.* **2009**, *34*, 431−448.

(12) Nakashima, T.; Kimizuka, N. Controlled self-assembly of amphiphiles in ionic liquids and the formation of ionogels by molecular tuning of cohesive energies. *Polym. J.* **2012**, *44*, 665−671.

(13) Visser, A. E.; Swatloski, R. P.; Griffin, S. T.; Hartman, D. H.; Rogers, R. D. Liquid/liquid extraction of metal ions in room temperature ionic liquids. *Sep. Sci. Technol.* **2001**, *36*, 785−804.

(14) Visser, A. E.; Swatloski, R. P.; Reichert, W. M.; Willauer, H. D.; Huddleston, J. G.; Rogers, R. D. In *Green Industrial Applications of Ionic Liquids*; Rogers, R. D., Seddon, K. R., Volkov, S., Eds.; Springer: New York, 2003; p 137−156.

(15) Anderson, J. L.; Pino, V.; Hagberg, E. C.; Sheares, V. V.; Armstrong, D. W. Surfactant solvation effects and micelle formation in ionic liquids. *Chem. Commun.* **2003**, 2444−2445.

(16) Evans, D. F.; Yamauchi, A.; Roman, R.; Casassa, E. Z. Micelle Formation in Ethylammonium Nitrate, a Low-Melting Fused Salt. *J. Colloid Interface Sci.* **1982**, *88*, 89−96.

(17) Greaves, T. L.; Drummond, C. J. Ionic liquids as amphiphile self-assembly media. *Chem. Soc. Rev.* **2008**, *37*, 1709−1726.

(18) Blanchard, L. A.; Hancu, D.; Beckman, E. J.; Brennecke, J. F. Green processing using ionic liquids and CO_2. *Nature* **1999**, *399*, 28−29.

(19) Walden, P. *Bull. Imp. Acad. Sci.* **1914**, 405−422.

(20) Greaves, T. L.; Drummond, C. J. Protic ionic liquids: Properties and applications. *Chem. Rev.* **2008**, *108*, 206−237.

(21) Evans, D. F.; Chen, S. H.; Schriver, G. W.; Arnett, E. M. Thermodynamics of Solution of Non-Polar Gases in a Fused Salt. Hydrophobic Bonding Behavior in a Non-Aqueous System. *J. Am. Chem. Soc.* **1981**, *103*, 481−482.

(22) Hayes, R.; Imberti, S.; Warr, G. G.; Atkin, R. The Nature of Hydrogen Bonding in Protic Ionic Liquids. *Angew. Chem., Int. Ed.* **2013**, *52*, 4623−4627.

(23) Atkin, R.; Warr, G. G. The smallest amphiphiles: Nanostructure in protic room-temperature ionic liquids with short alkyl groups. *J. Phys. Chem. B* **2008**, *112*, 4164−4166.

(24) Gohy, J. F. Block copolymer micelles. *Adv. Polym. Sci.* **2005**, *190*, 65−136.

(25) Tanford, C. Micelle Shape and Size. *J. Phys. Chem.* **1972**, *76*, 3020−3024.

(26) Israelachvili, J. N.; Mitchell, D. J.; Ninham, B. W. Theory of Self-Assembly of Hydrocarbon Amphiphiles into Micelles and Bilayers. *J. Chem. Soc., Faraday Trans. 2* **1976**, *72*, 1525−1568.

(27) Rodriguez-Hernandez, J.; Checot, F.; Gnanou, Y.; Lecommandoux, S. Toward 'smart' nano-objects by self-assembly of block copolymers in solution. *Prog. Polym. Sci.* **2005**, *30*, 691−724.

(28) Gaucher, G.; Dufresne, M.-H.; Sant, V. P.; Kang, N.; Maysinger, D.; Leroux, J.-C. Block copolymer micelles: Preparation, character-

DOI: 10.1021/acs.langmuir.5b01500
Langmuir 2015, 31, 7025−7031

ization and application in drug delivery. *J. Controlled Release* **2005**, *109*, 169−188.
(29) Kwon, G. S.; Kataoka, K. Block copolymer micelles as long-circulating drug vehicles. *Adv. Drug Delivery Rev.* **2012**, *64*, 237−245.
(30) Schacher, F. H.; Rupar, P. A.; Manners, I. Functional Block Copolymers: Nanostructured Materials with Emerging Applications. *Angew. Chem., Int. Ed.* **2012**, *51*, 7898−7921.
(31) Zhao, D. Y.; Huo, Q. S.; Feng, J. L.; Chmelka, B. F.; Stucky, G. D. Nonionic triblock and star diblock copolymer and oligomeric surfactant syntheses of highly ordered, hydrothermally stable, mesoporous silica structures. *J. Am. Chem. Soc.* **1998**, *120*, 6024−6036.
(32) Topolnicki, I. L.; FitzGerald, P. A.; Atkin, R.; Warr, G. G. Effect of Protic Ionic Liquid and Surfactant Structure on Partitioning of Polyoxyethylene Non-ionic Surfactants. *ChemPhysChem* **2014**, *15*, 2485−2489.
(33) Araos, M. U.; Warr, G. G. Self-Assembly of Nonionic Surfactants into Lyotropic Liquid Crystals in Ethylammonium Nitrate, a Room-Temperature Ionic Liquid. *J. Phys. Chem. B* **2005**, *109*, 14275−14277.
(34) Hoarfrost, M. L.; Lodge, T. P. Effects of Solvent Quality and Degree of Polymerization on the Critical Micelle Temperature of Poly(ethylene oxide-*b*-*n*-butyl methacrylate) in Ionic Liquids. *Macromolecules* **2014**, *47*, 1455−1461.
(35) López-Barrón, C. R.; Li, D.; Wagner, N. J.; Caplan, J. L. Triblock Copolymer Self-Assembly in Ionic Liquids: Effect of PEO Block Length on the Self-Assembly of PEO−PPO−PEO in Ethylammonium Nitrate. *Macromolecules* **2014**, *47*, 7484−7495.
(36) Mansfeld, U.; Hoeppener, S.; Schubert, U. S. Investigating the Motion of Diblock Copolymer Assemblies in Ionic Liquids by in Situ Electron Microscopy. *Adv. Mater. (Weinheim, Ger.)* **2013**, *25*, 761−765.
(37) He, Y. Y.; Li, Z. B.; Simone, P.; Lodge, T. P. Self-assembly of block copolymer micelles in an ionic liquid. *J. Am. Chem. Soc.* **2006**, *128*, 2745−2750.
(38) Lee, H.-N.; Bai, Z.; Newell, N.; Lodge, T. P. Micelle/Inverse Micelle Self-Assembly of a PEO-PNIPAm Block Copolymer in Ionic Liquids with Double Thermoresponsivity. *Macromolecules* **2010**, *43*, 9522−9528.
(39) Lu, H. Y.; Akgun, B.; Wei, X. Y.; Li, L.; Satija, S. K.; Russell, T. P. Temperature-Triggered Micellization of Block Copolymers on an Ionic Liquid Surface. *Langmuir* **2011**, *27*, 12443−12450.
(40) Vekariya, R. L.; Ray, D.; Aswal, V. K.; Hassan, P. A.; Soni, S. S. Effect of ionic liquids on microstructures of micellar aggregates-formed by PEO-PPO-PEO block copolymer in aqueous solution. *Colloid Surf., A* **2014**, *462*, 153−161.
(41) Virgili, J. M.; Hoarfrost, M. L.; Segalman, R. A. Effect of an Ionic Liquid Solvent on the Phase Behavior of Block Copolymers. *Macromolecules* **2010**, *43*, 5417−5423.
(42) Sharma, S. C.; Atkin, R.; Warr, G. G. The Effect of Ionic Liquid Hydrophobicity and Solvent Miscibility on Pluronic Amphiphile Self-Assembly. *J. Phys. Chem. B* **2013**, *117*, 14568−14575.
(43) Simone, P. M.; Lodge, T. P. Lyotropic Phase Behavior of Polybutadiene−Poly(ethylene oxide) Diblock Copolymers in Ionic Liquids. *Macromolecules* **2008**, *41*, 1753−1759.
(44) Ueki, T.; Watanabe, M. Polymers in Ionic Liquids: Dawn of Neoteric Solvents and Innovative Materials. *Bull. Chem. Soc. Jpn.* **2012**, *85*, 33−50.
(45) Batrakova, E. V.; Kabanov, A. V. Pluronic block copolymers: Evolution of drug delivery concept from inert nanocarriers to biological response modifiers. *J. Controlled Release* **2008**, *130*, 98−106.
(46) Chen, S.; Guo, C.; Liu, H. Z.; Wang, J.; Liang, X. F.; Zheng, L.; Ma, J. H. Thermodynamic analysis of micellization in PEO−PPO−PEO block copolymer solutions from the hydrogen bonding point of view. *Mol. Simul.* **2006**, *32*, 409−418.
(47) Goldmints, I.; von Gottberg, F. K.; Smith, K. A.; Hatton, T. A. Small-Angle Neutron Scattering Study of PEO−PPO−PEO Micelle Structure in the Unimer-to-Micelle Transition Region. *Langmuir* **1997**, *13*, 3659−3664.
(48) Atkin, R.; De Fina, L. M.; Kiederling, U.; Warr, G. G. Structure and Self Assembly of Pluronic Amphiphiles in Ethylammonium Nitrate and at the Silica Surface. *J. Phys. Chem. B* **2009**, *113*, 12201−12213.
(49) Zhang, G. D.; Chen, X.; Zhao, Y. R.; Ma, F. M.; Jing, B.; Qiu, H. Y. Lyotropic liquid-crystalline phases formed by Pluronic P123 in ethylammonium nitrate. *J. Phys. Chem. B* **2008**, *112*, 6578−6584.
(50) Bodratti, A. M.; Sarkar, B.; Song, D. D.; Tsianou, M.; Alexandridis, P. Competitive Adsorption Between PEO-Containing Block Copolymers and Homopolymers at Silica. *J. Dispersion Sci. Technol.* **2015**, *36*, 1−9.
(51) Liu, X.; Wu, D.; Turgman-Cohen, S.; Genzer, J.; Theyson, T. W.; Rojas, O. J. Adsorption of a Nonionic Symmetric Triblock Copolymer on Surfaces with Different Hydrophobicity. *Langmuir* **2010**, *26*, 9565−9574.
(52) Hamley, I. W.; Connell, S. D.; Collins, S. In Situ Atomic Force Microscopy Imaging of Adsorbed Block Copolymer Micelles. *Macromolecules* **2004**, *37*, 5337−5351.
(53) Kodama, K.; Tsuda, R.; Niitsuma, K.; Tamura, T.; Ueki, T.; Kokubo, H.; Watanabe, M. Structural effects of polyethers and ionic liquids in their binary mixtures on lower critical solution temperature liquid-liquid phase separation. *Polym. J.* **2011**, *43*, 242−248.
(54) Ogura, M.; Tokuda, H.; Imabayashi, S. I.; Watanabe, M. Preparation and solution behavior of a thermoresponsive diblock copolymer of poly(ethyl glycidyl ether) and poly(ethylene oxide). *Langmuir* **2007**, *23*, 9429−9434.
(55) Ueki, T.; Watanabe, M.; Lodge, T. P. Doubly Thermosensitive Self-Assembly of Diblock Copolymers in Ionic Liquids. *Macromolecules* **2009**, *42*, 1315−1320.
(56) Chen, Z.; FitzGerald, P. A.; Kobayashi, Y.; Ueno, K.; Watanabe, M.; Warr, G. G.; Atkin, R. Micelle Structure of Novel Diblock Polyethers in Water and Two Protic Ionic Liquids (EAN and PAN). *Macromolecules* **2015**, *48*, 1843−1851.
(57) Werzer, O.; Warr, G. G.; Atkin, R. Conformation of Poly(ethylene oxide) Dissolved in Ethylammonium Nitrate. *J. Phys. Chem. B* **2011**, *115*, 648−652.
(58) Haupt, B. J.; Senden, T. J.; Sevick, E. M. AFM Evidence of Rayleigh Instability in Single Polymer Chains. *Langmuir* **2002**, *18*, 2174−2182.
(59) Elbourne, A.; Voitchovsky, K.; Warr, G. G.; Atkin, R. Ion structure controls ionic liquid near-surface and interfacial nanostructure. *Chem. Sci.* **2015**, *6*, 527−536.
(60) Atkin, R.; Warr, G. G. Structure in Confined Room-Temperature Ionic Liquids. *J. Phys. Chem. C* **2007**, *111*, 5162−5168.

DOI: 10.1021/acs.langmuir.5b01500
Langmuir 2015, 31, 7025−7031